Journal of Magnetic Resonance 309 (2019) 106624

Contents lists available at ScienceDirect

Journal of Magnetic Resonance

journal homepage: www.elsevier.com/locate/jmr

Direct NMR T_1 distribution measurement without using ill-posed fitting methods

E.T. Montrazi *, T.J. Bonagamba

São Carlos Institute of Physics, University of São Paulo, PO Box 369, 13560-970 São Carlos, SP, Brazil

ARTICLE INFO

Article history:
Received 18 July 2019
Revised 17 October 2019
Accepted 20 October 2019
Available online 22 October 2019

Keywords:
NMR
Spin-lattice relaxation
T_1 distribution
Combined saturation-inversion-recovery
SIR
Direct T_1 distribution measurement by SIR
DSIR-T_1

ABSTRACT

The usual Nuclear Magnetic Resonance (NMR) experiments for measuring spin–lattice relaxation time (T_1) distributions are Inversion-Recovery (IR) and Saturation-Recovery (SR), followed by data processing based on ill-posed multi-exponential curve fitting methods. Recently, a new method combining SR and IR, called Saturation-Inversion-Recovery (SIR), has been proposed to obtain sharper T_1-dependences than IR and SR. In this article, we propose an appropriate combination of SIR signals to directly obtain T_1 distributions without using any multi-exponential fitting methods.

1. Introduction

The most traditional Nuclear Magnetic Resonance (NMR) experiments for measuring spin-lattice relaxation time (T_1) are Inversion-Recovery (IR) and Saturation-Recovery (SR) experiments [1,2].

In 2012, a method was proposed combining SR and IR, called Hybrid Saturation-Inversion-Recovery (HSIR), where the time between Saturation and Inversion was kept constant, allowing an efficient T_1 measurement, with the advantage of avoiding the waiting time to repolarize the magnetization [3].

In 2017, a new combination of SR and IR, called Saturation-Inversion-Recovery (SIR), was proposed to obtain sharper T_1-dependences than those obtained by IR and SR [4]. In this article, authors demonstrated that SIR is a good tool for NMR studies involving samples presenting broad T_1 distributions, such as porous and biological samples.

In most of the studied materials, such as porous media, measurements involve T_1 distributions. The usual procedure for obtaining T_1 distributions involves data processing based on ill-posed multi-exponential curve fitting methods, such as Inverse Laplace Transform (ILT), which brings uncertainty to the interpretation of NMR data [5–8].

In this article, we propose an appropriate combination of SIR signals to directly obtain T_1 distributions without using any kind of multi-exponential fitting method. We call this new method "Direct T_1 Distribution Measurement by SIR", using the acronym DSIR-T_1.

2. Proposed method

The Saturation-Inversion-Recovery (SIR) pulse sequence and experiment are described in detail in Ref. [4]. This experiment can be run with several inversion steps, saturation-[$n \times$ inversion]-recovery, where n is the number of π pulses. In this case, the pulse sequence is called SIRN. The signal obtained from SIRN is given by [5]:

$$S^n_{sir}(t) = \sum_{i=0}^{n} (-1)^i (1-A) A^i, \quad (1)$$

where $A = e^{-t/T_1}$.

After carrying out the SIRN experiments for different n values, the observed signals can be combined as follows:

$$S^p(t) = \sum_{n=0}^{p} \alpha_n S^n_{sir}(t) = \sum_{j=0}^{p+1} a_j A^j, \quad (2)$$

where the α_n values can be chosen appropriately to obtain the desired a_j and A^j values.

* Corresponding author.
E-mail address: elton.montrazi@usp.br (E.T. Montrazi).

https://doi.org/10.1016/j.jmr.2019.106624
1090-7807/

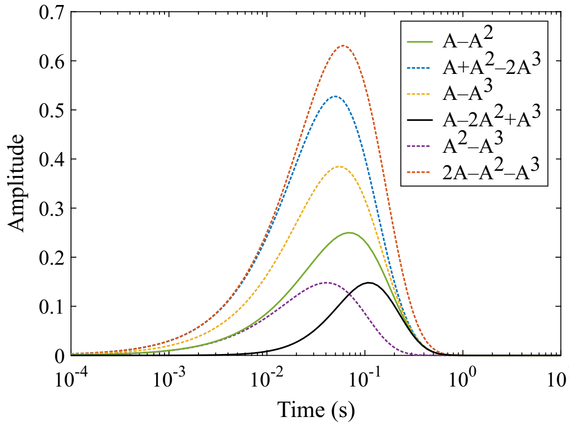

Fig. 1. Peak-shaped functions obtained for $p = 2$ and $a_j's$ ranging between -2 and 2. A-A^2 is the only solution for $p = 1$ and A-2A^2 + A^3 is the narrower peak-shaped function, when $p = 2$.

Using Eq. (2), the terms a_j and A^j can be combined to obtain a peak-shaped function. To demonstrate this, we constructed several peak-shaped functions using Eq. (2) for $T_1 = 0.1$ s and t ranging between 10^{-4} and 10 s (100 logarithmically spaced values). Fig. 1 shows several appropriate combinations of a_j and A^j that result in peak-shaped functions for $p = 2$, with $a_j's$ ranging between -2 and 2.

As shown in Fig. 1, there are many possibilities to obtain a peak-shaped function. However, it can be shown that the narrower peak-shaped functions occur, for each p-value, when the $a_j's$ values follow the binomial theorem (Pascal's triangle):

$$S^1(t) = A - A^2 \tag{3}$$

$$S^2(t) = A - 2A^2 + A^3 \tag{4}$$

$$S^3(t) = A - 3A^2 + 3A^3 - A^4 \tag{5}$$

$$S^4(t) = A - 4A^2 + 6A^3 - 4A^4 + A^5 \tag{6}$$

$$S^5(t) = A - 5A^2 + 10A^3 - 10A^4 + 5A^5 - A^6 \tag{7}$$

and so on.

Eqs. (3)–(7) can be written in the following compact form:

$$S^p_{T_1}(t) \equiv S^p_{DSIR-T_1}(t) = A(1 - A)^p, \tag{8}$$

where the peak-shaped functions correspond to the product of exponential growth and decay functions.

Using a simple calculation, we determined the coefficients of the sum of the SIRN signals, $\alpha_n's$ in Eq. (2), that results in $S^p_{T_1}$'s, Eqs. (3) to (7):

$$S^1_{T_1}(t) = S^0_{sir}(t) - S^1_{sir}(t) \tag{9}$$

$$S^2_{T_1}(t) = S^0_{sir}(t) - S^2_{sir}(t) \tag{10}$$

$$S^3_{T_1}(t) = S^0_{sir}(t) + S^1_{sir}(t) - S^2_{sir}(t) - S^3_{sir}(t) \tag{11}$$

$$S^4_{T_1}(t) = S^0_{sir}(t) + 2S^1_{sir}(t) - 2S^3_{sir}(t) - S^4_{sir}(t) \tag{12}$$

$$S^5_{T_1}(t) = S^0_{sir}(t) + 3S^1_{sir}(t) + 2S^2_{sir}(t) - 2S^3_{sir}(t) - 3S^4_{sir}(t) - S^5_{sir}(t) \tag{13}$$

and so on. The conclusion is that $\alpha_n's$ follow the Pascal's triangle rule with the initial condition 1 and -1.

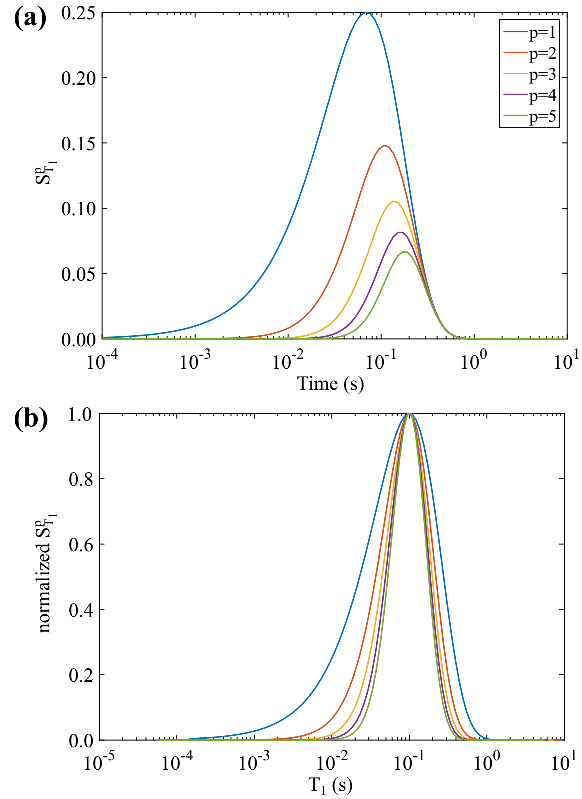

Fig. 2. (a) The $S^p_{T_1}$ amplitude reduces in function of p, as shown for the first five. (b) The five first normalized $S^p_{T_1}$ in which the time scale was transformed to T_1 scale by using Eq. (14). Note that the distribution width reduces *vs. p*.

Fig. 2a shows the five first $S^p_{T_1}$ (Eqs. (3)–(7)). The larger the p, the narrower the $S^p_{T_1}$, meaning higher resolution in T_1 distribution and lower amplitude.

Since $S^p_{T_1}$ is a peak-shaped function in the time domain, it is necessary to transform the time scale to that of T_1. This can be done by deriving $S^p_{T_1}$ with respect to t, where the maximum of this function occurs when

$$t = T_1 \ln(1 + p) \tag{14}$$

Fig. 2b illustrates the scale transformation from t to T_1 using Eq. (14). In the transformed scale, the five first $S^p_{T_1}$ were normalized to emphasize that the width reduces for larger p. Despite having higher resolution in T_1 for larger p, this imposes a smaller amplitude for $S^p_{T_1}$, as well as a lower signal-to-noise ratio in the T_1 distribution. Note that $S^p_{T_1}$'s are not perfectly symmetrical.

In the simulation of $S^p_{T_1}$, for$p = 3$ and three T_1 values, 0.01, 0.1, and 1 s, we obtain a distribution with 3 peaks (line in black in Fig. 3a). This signal corresponds to the sum of each $S^p_{T_1}$ for each T_1 value, separately (lines in yellow, red and blue in Fig. 3a). Note that in the log-scale, the width of $S^p_{T_1}$ is independent of the T_1 value.

In the case where the T_1values are close, i.e. 0.05, 0.1 and 0.2 s in Fig. 3b, the $S^p_{T_1}$ of each T_1 overlaps so that we cannot perfectly distinguish the 3 peaks in the T_1 distribution. Thus, we need to define a resolution criterion for the method. Several criteria could be used for this purpose, for example, Rayleigh criterion in the field of optics [9]. Here, the distribution is considered to be resolved when the half-intensity point of a peak, x^{η}_2, is at most equal to the half-intensity point of a neighbor peak, x^{σ}_1, as illustrated in Fig. 4.

x_1^η and x_2^η are proportional to T_1^η, $x_1^\eta = c_1 T_1^\eta$ and $x_2^\eta = c_2 T_1^\eta$, where c_1 and c_2 are constants independent of T_1^η. The constants c_1 and c_2 were numerically calculated and the values are presented in Table 1. Thus, for the criterion $x_2^\eta = x_1^\sigma$, we obtain

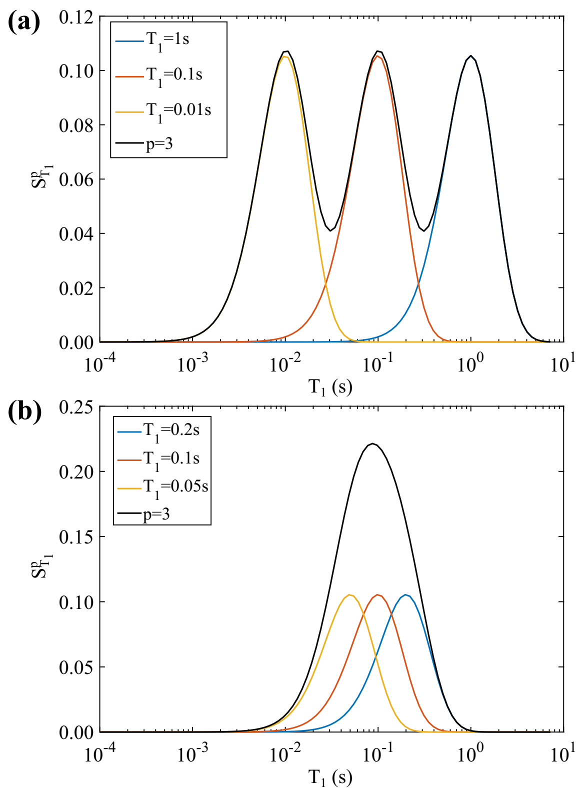

Fig. 3. (a) $S_{T_1}^3$, line in black, for 3 T_1 values. $S_{T_1}^3$ corresponds to the sum of each $S_{T_1}^3$ for each T_1 value, separately (lines in yellow, red and blue). (b) When the T_1 values are near, the $S_{T_1}^3$ for each T_1 overlaps and the 3 peaks cannot be perfectly distinguished in the T_1 distribution. (For interpretation of the references to colour in this figure legend, the reader is referred to the web version of this article.)

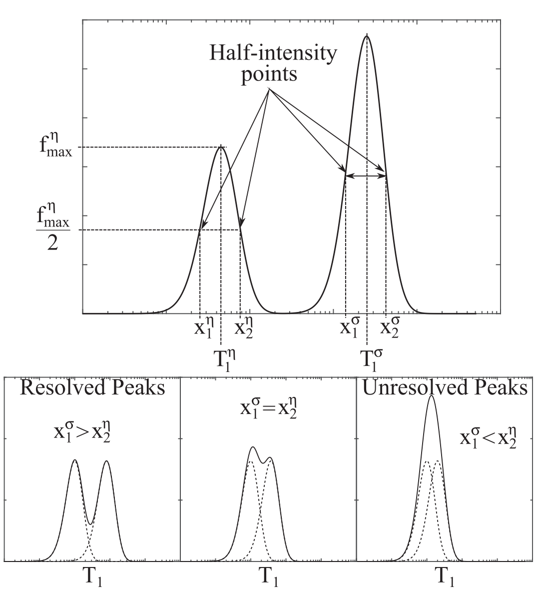

Fig. 4. Illustration of the cases where two peaks are resolved and unresolved. The criterion to minimum resolution is when the half-intensity point of a peak (x_2^η) is equal to the half-intensity point of the other peak (x_1^σ).

$$\frac{T_1^\sigma}{T_1^\eta} = \frac{x_1^\sigma / c_1}{x_2^\eta / c_2} = \frac{c_2}{c_1} \tag{15}$$

From Eq. (15), we conclude that two peaks can be considered resolved when the ratio between two consecutive T_1 values is greater than the ratio c_2 to c_1, which is presented in Table 1.

Because $S_{T_1}^p$'s are not perfectly symmetrical, when the two peaks are in the minimum resolution, the T_1 distribution is deformed. As already mentioned, the greater the p, the smaller the c_2/c_1, and, consequently, the higher the resolution of the T_1 distribution. Changing p from 1 to 2, results in a significant increase in the resolution. However, for $p > 10$, we need to greatly increase this parameter to improve the resolution. In this case, it is important to point out that the greater the p, the longer the experiment, making it not viable.

Table 1
The table presents the constants c_1 and c_2 to obtain the half-intensity points of the peaks, and the ratio c_2/c_1 that is connected with the resolution of the T_1 distribution.

k	$c_1 = x_1/T_1$	$c_2 = x_2/T_1$	c_2/c_1
1	0.23	2.77	12.04
2	0.37	2.20	5.95
3	0.44	1.98	4.50
4	0.49	1.86	3.80
5	0.53	1.78	3.36
10	0.62	1.59	2.56
100	0.79	1.32	1.67
1000	0.86	1.21	1.41
10,000	0.89	1.16	1.30

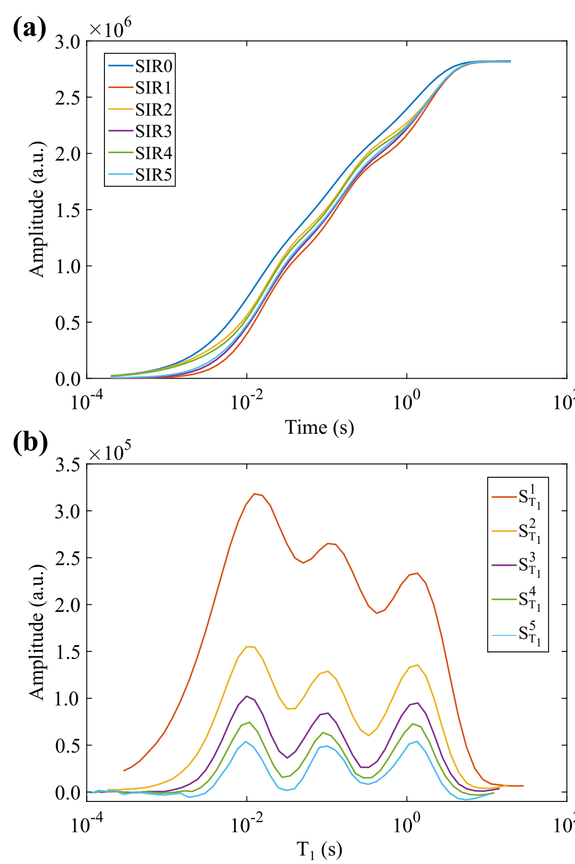

Fig. 5. (a) SIRN signal from the system comprising three $CuSO_4$ solutions. (b) T_1 distributions obtained from (a) by the peak-shaped function method (Eq. (8)).

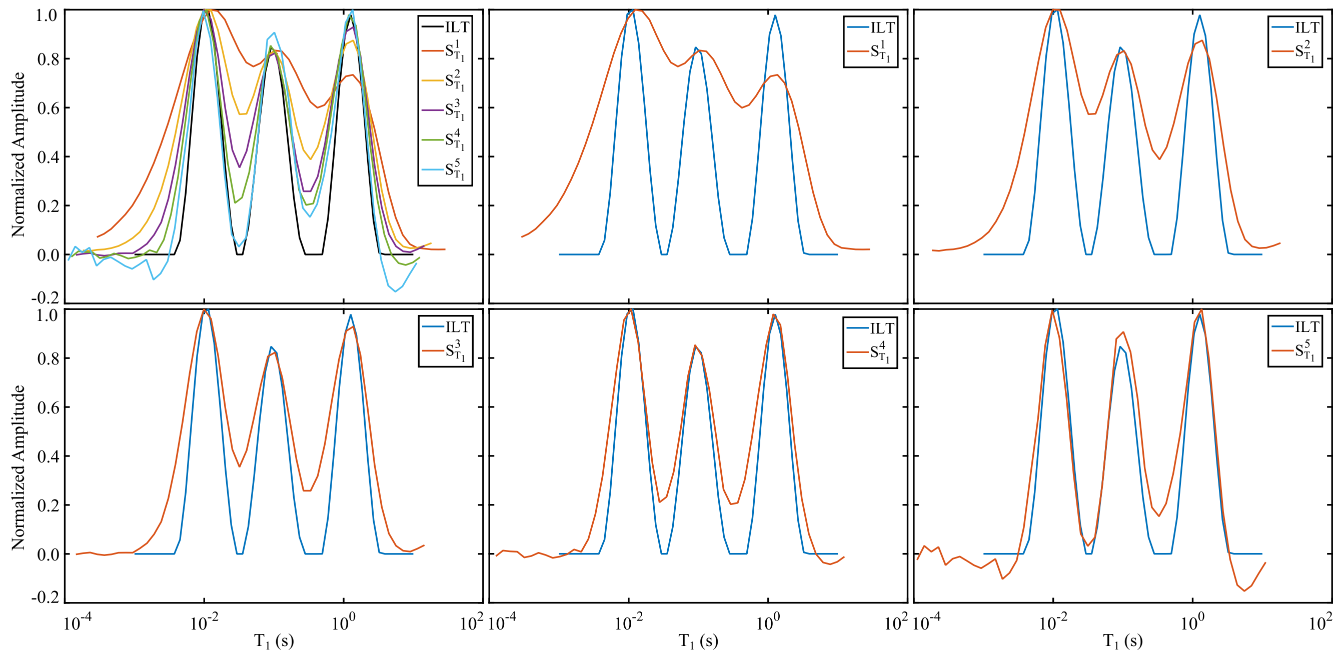

Fig. 6. Normalized T_1 distributions obtained by the DSIR-T$_1$ (Fig. 5b) and ILT (by UPEN) methods. $S^p_{T_1}$'s are in agreement with the ILT result.

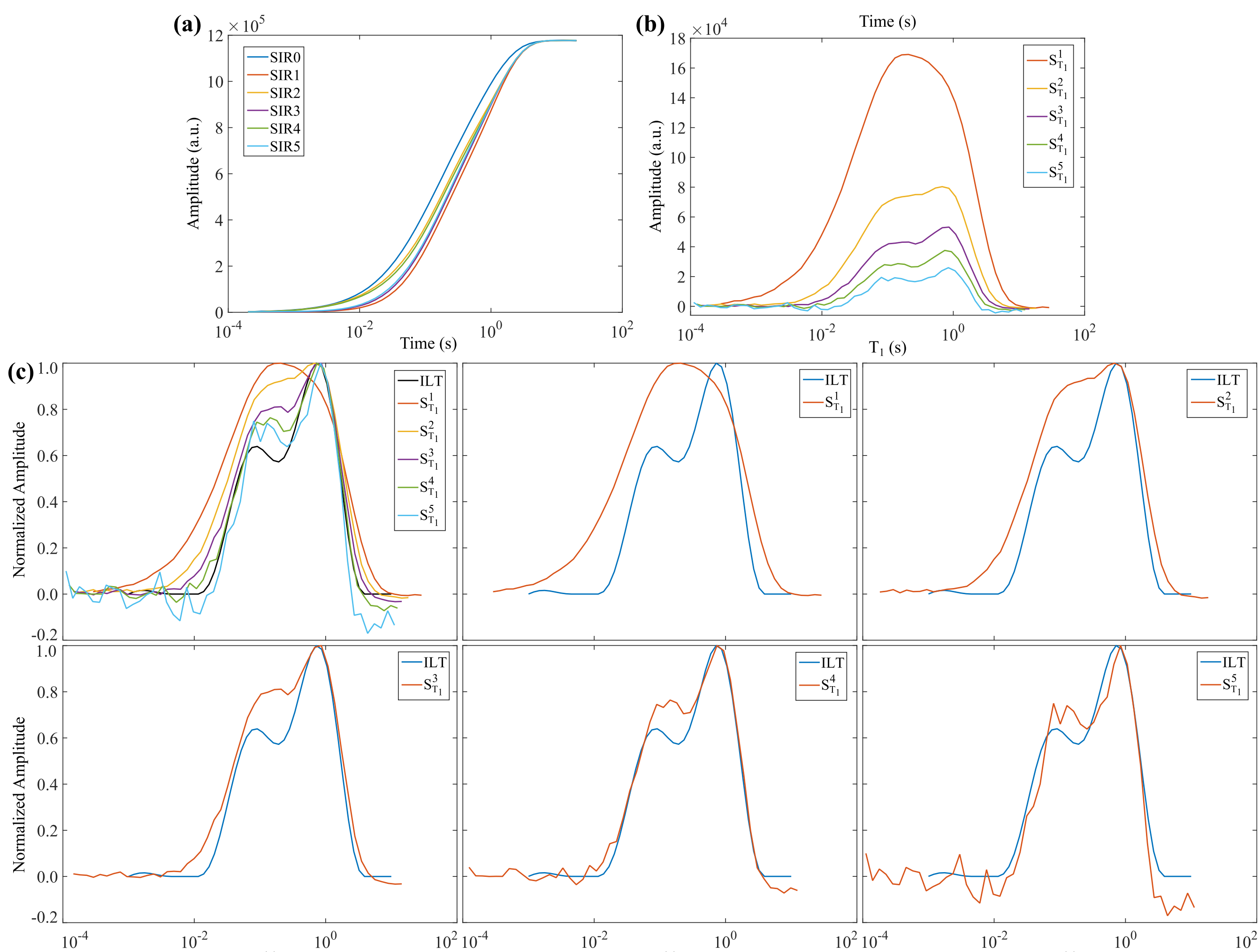

Fig. 7. (a) The SIRN signals from the CWL sample. (b) Correspondent T_1 distributions obtained by the DSIR-T$_1$ method. (c) Comparison between normalized T_1 distributions obtained by the DSIR-T$_1$ and ILT (by UPEN) methods for CWL.

3. Results and discussions

The SIRN experiment, $Sat. - \tau - n \times \left[180^{\circ} - \tau\right] - 90^{\circ} - Acq.$, has already been well described in the paper where it was proposed [4]. In this work, we ran the sequences for $n = 0$ to 5 (Eqs. (3)–(7)) and obtained $S^{p}_{T_1}$ for p = 1–5 through Eq. (4) (Eqs. (9) to (13)). To compare with the DSIR-T_1 method, we used an ILT method called Uniform Penalty (UPEN) algorithm [6].

The SIRN experiments were performed in two samples at room temperature. The first one comprised three NMR tubes filled with different solutions of $CuSO_4$: ~1, ~10, and ~100 mM. The second one consisted of a water saturated sedimentary rock (Portland Coombefield Whitbed Limestone (CWL) [10]).

The experiments were performed using an Oxford 2 T superconducting magnet (^{1}H Larmor frequency of 85 MHz) controlled by a TECMAG Redstone spectrometer.

The magnetization saturation was done by applying a radiofrequency (rf) pulse of 200 ms. The calibration of 180° and 90° pulses resulted in pulse lengths of approximated 20 µs (same length for the 90° pulse by reducing the rf power by a quarter). 50 logarithmic spaced values from 200 µs to 20 s were chosen for the magnetization evolution time τ. In order to obtain better results using the proposed technique, we used composite pulses $90°_x180°_{-y}90°_x$ for magnetization inversion. Phase cycling was done just for 90° of the excitation pulse and acquisition (x, y, −x, −y), resulting in 12 scans.

Fig. 5 shows the SIRN signals (Fig. 5a) and $S^{p}_{T_1}$'s (Fig. 5b) obtained from the system composed of three $CuSO_4$ solutions. As expected, we can observe three peaks, which have the maximum at approximated 0.01, 0.1 and 1 s. As discussed in the simulation section, Fig. 2, the amplitude of $S^{p}_{T_1}$ reduced as a function of p.

In Fig. 6, $S^{p}_{T_1}$'s were normalized and compared with the corresponding data obtained by the ILT method. A satisfactory match can be observed between the methods, mainly for larger p-values, as already mentioned.

The results obtained for water saturated Portland Coombefield Whitbed Limestone (CWL) are presented in Fig. 7. For $p = 1$, due to the expected lower resolution, it is difficult to identify the number of peaks in the T_1 distributions. For larger p-values, the resolution increases and the results obtained by the DSIR-T_1 and ILT methods are closer.

Figs. 6 and 7 clearly show that the experimental results obtained by the proposed method are very promising and agree with the results obtained traditionally via ILT. Consequently, the DSIR-T_1 method is a complementary or substitute option for the ill-posed ILT method.

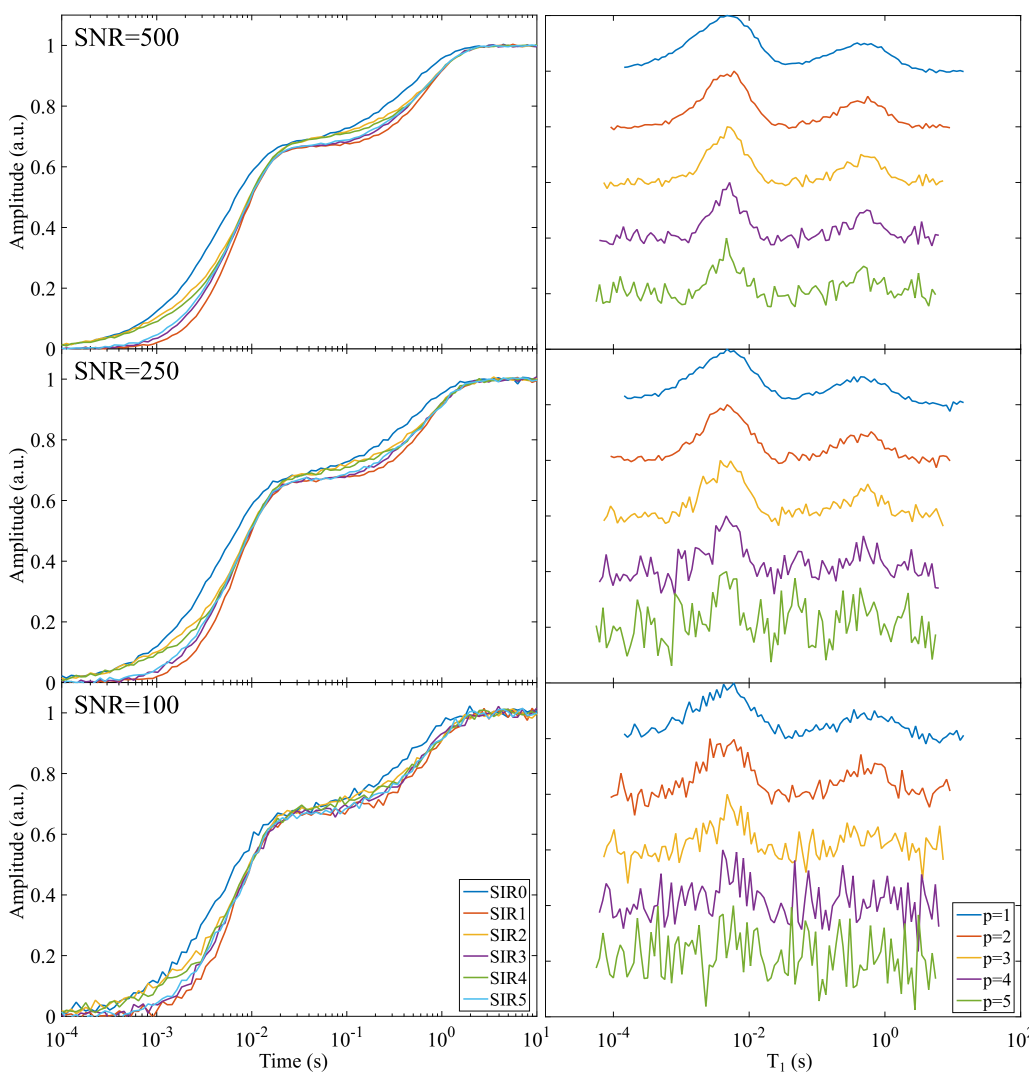

Fig. 8. Simulated SIRN signals with different signal-to-noise ratios (SNR) and the respective $S^{p}_{T_1}$'s. Depending on the desired p-value, a minimum of SNR is required.

Each point in SIRN is given by the FID amplitude. The FID signal, for each scan, presented a signal-to-noise ratio (SNR) of 640 and 390 for phantom and CWL samples, respectively (SNR was calculated by the maximum of the signal divided by the root mean square of the end of FID, where there is no longer an NMR signal). The SIRN experiments were run in sequence (SIR0 to SIR5) for each scan. The SIRN signals for the 12 scans, Figs. 6a and 8a, resulted in an SNR of approximately 3000 (the SNR was calculated by the maximum of the SIRN signal divided by the root mean square of the end of this signal, removing the offset).

For the five first DSIR-T_1 signals, the amplitudes are approximately 0.25, 0.15, 0.1, 0.08, and 0.06, for SIRN with amplitude 1, Fig. 2a. The noise is summed n times, depending on the coefficients of the sum (Eqs. (9)–(13)): 2, 2, 4, 6, and 12 times for the first five DSIR-T_1, respectively. The effect of summing noises can be observed in the DSIR-T_1 distributions, Figs. 6 and 7.

To verify the influence of noise in $S^p_{T_1}$, two peaks with T_1 equal 0.005 and 0.5 s with amplitudes 2 to 1, respectively, were simulated for different signal-to-noise ratios (SNR). As can be seen in Fig. 8, for SIRN signals with SNR = 500, the two peaks are resolved for the five $p's$. On the other hand, for SNR = 250, the second peak in $S^5_{T_1}$ is above the noise, and for SNR = 100, we can observe that for $S^5_{T_1}$ and $S^4_{T_1}$ the signals are not distinguished from noise. This indicates that the SNR limits the p-value that we can use for DSIR experiments.

4. Conclusions

This work proposes a new method that obtains T_1 distributions without using the ill-posed ILT method. The method is based on the appropriate combination of Saturation-Inversion-Recovery (SIR) experiments. The method was fully tested using real samples with convincing experimental results compared to those obtained with ILT. It can be used as a complement or substitute for the ill-posed ILT method, especially when there are doubts about the method of adjustment, such as choosing the regularization parameter.

Declaration of Competing Interest

The authors declare that they have no known competing financial interests or personal relationships that could have appeared to influence the work reported in this paper.

Acknowledgements

This study was financed in part by the Coordenação de Aperfeiçoamento de Pessoal de Nível Superior - Brasil (CAPES) - Finance Code 001, Conselho Nacional de Desenvolvimento Científico e Tecnológico - Brasil (CNPq), Fundação de Amparo à Pesquisa do Estado de São Paulo – Brasil (FAPESP) (Project: 2009/54880-6), Agência Nacional do Petróleo - Petrobras - Brasil (ANP) (Projects: 2012/00380-5 and 2015/00416-8), and the Universidade de São Paulo (USP).

References

[1] R. Kleinberg, Encyclopedia of Nuclear Magnetic Resonance, Wiley, New York, USA, 1995.
[2] M.H. Levitt, Spin Dynamics. Basics of Nuclear Magnetic Resonance, Wiley, Chichester, UK, 2001.
[3] L. Li, S. Chen, Sensitive New NMR Hybrid T1 Measurements for Gas Shale, Heavy Oil, and Microporosity Characterizations. Society of Petroleum Engineers, SPE-158833-MS, January 1 2012.
[4] H. Wang, M. Zhao, J.L. Askerman, Y.-Q. Song, Saturation-inversion-recovery: a method for T_1 measurement, J. Magnet. Reson. 274 (2017) 137–143.
[5] A.A. Istratov, O.F. Vyvenko, Exponential analysis in physical phenomena, Rev. Sci. Instrum. 70 (1999) 1233.
[6] G.C. Borgia, R.J.S. Brown, P. Fantazzini, Uniform-penalty inversion of multiexponential decay data, J. Magnet. Reson. 132 (1998) 65–77.
[7] Y.-Q. Song, L. Venkataramanan, L. Burcaw, Determining the resolution of Laplace inversion spectrum, J. Chem. Phys. 122 (2005) 104104.
[8] Y.-Q. Song, Resolution and uncertainty of Laplace inversion spectrum, Magn. Reson. Imag. 25 (2007) 445–448.
[9] F.R.S. Lord Rayleigh, Investigations in optics, with special reference to the spectroscope, Phil. Mag. 5, 8 49 (1879) 261–274.
[10] E.T. Montrazi, T.J. Bonagamba, Saturation-recovery as a T_1-filter for T_2–T_2 exchange NMR, J. Magn. Reson. 301 (2019) 67–72.